Ferrocene functionalized multi-walled carbon nanotubes as supercapacitor electrodes

Gomaa A.M. Ali [a,*], Elżbieta Megiel [b,*], Piotr Cieciórski [b], Mohammad R. Thalji [c], Jan Romański [b], H. Algarni [d,e], Kwok Feng Chong [c,*]

[a] Chemistry Department, Faculty of Science, Al–Azhar University, Assiut 71524, Egypt
[b] University of Warsaw, Faculty of Chemistry, Pasteura 1, 02-093 Warsaw, Poland
[c] Faculty of Industrial Sciences & Technology, Universiti Malaysia Pahang, Gambang, 26300 Kuantan, Malaysia
[d] Research Centre for Advanced Materials Science (RCAMS), King Khalid University, Abha 61413, P. O. Box 9004, Saudi Arabia
[e] Department of Physics, Faculty of Sciences, King Khalid University, P. O. Box 9004, Abha, Saudi Arabia

ARTICLE INFO

ABSTRACT

Modified multi-walled carbon nanotubes (MWCNTs) functionalized by a redox-active ferrocene (Fc-MWCNTs) were successfully synthesized to enhance the electrochemical performance of MWCNTs for supercapacitor application. The ferrocene moieties were attached to the surface of MWCNTs *via* a thiourea linker with anions-interacting capability. The Fc-MWCNTs were characterized using XPS, FTIR, SEM, TGA, DTG, and XRF methods. The electrochemical performance details were investigated using cyclic voltammetry, galvanostatic charge-discharge, and electrochemical impedance spectroscopy. The Fc-MWCNTs electrode showed excellent capacity retention (90.8% over 5000 cycles) and a specific capacitance of $50\,F\,g^{-1}$ at $0.25\,A\,g^{-1}$ that is several times higher as compared to the pristine MWCNTs. The fabricated Fc-MWCNTs is proposed to be a suitable and promising candidate for energy storage material.

© 2020 Published by Elsevier B.V.

1. Introduction

Over the last three decades, the functionalization of carbon nanotubes (CNTs) by electroactive moieties attracts considerable attention due to its performance enhancement in electronic applications and also opening up new opportunities for their use [1–5]. Ferrocene (Fc) is a well-known redox-active compound that can be used as an effective electron-transfer mediator [6,7]. Low oxidation potential, the stability of its redox states, and well-known electrochemical behaviour make it an ideal redox-active molecule model often to be used as redox probes and modifiers [8,9].

Noncovalent functionalization of single-walled carbon nanotubes (SWCNTs) with Fc was reported by Yang et al. [10]. Interestingly, they observed the cooperative effect between Fc and CNTs due to the π-π stacking interactions gives a dramatically enhanced electrochemical property of the fabricated material. This phenomenon was explained by the accelerated electron transfer through the π-π stacking interactions between Fc and SWCNTs [10]. Guan et al. [11] reported the fabrication of ferrocene-modified single-walled carbon nanotubes (SWCNTs) in which the ferrocene molecules were trapped inside of

hollow space of the nanotubes. This nanohybrid material may act as an air-stable *n*-type field-effect transistor and constitute a building block for various devices [11]. Whereas, Prato and co-workers [12] had proven that in the case of SWCNTs, which its surface was covalently functionalized with ferrocene, the photoinduced electron transfer occurs under the influence of visible light. The electron transfer leads to the formation of long-lived SWCNT•⁻-Fc•⁺ species. This phenomenon seems to be very promising in light of the application for solar-energy conversion devices. Fc is also a convenient signalling unit commonly used in the field of supramolecular chemistry and construction of anion and ion pair receptors.

By incorporation of the Fc unit in the proximity of binding domains anion [13–16] and ion pair sensors [17–24], it is capable of tracking the binding event by electrochemical measurements. We envision that this protocol could be utilized in the preparation of SWCNTs modified with Fc-based anion receptors. In the reaction of isothiocyanatoferrocene with SWCNTs containing amino groups, it can attach Fc moiety to the solid support in addition to the thiourea's function to interact with anions. This leads to electroactive material whose properties will be affected by the presence of anions. The addition of Fc moiety was also proven to alter the surface properties as the SiO_2 was changed from hydrophobic into hydrophilic with the addition of Fc [25]. Similar to iron-containing Fc moiety, introducing other iron-containing moieties into MWCNTs was found to increase the hydrophilic characteristics [26].

* Corresponding authors.
  E-mail addresses: gomaasanad@azhar.edu.eg (G.A.M. Ali), emegiel@chem.uw.edu.pl (E. Megiel), ckfeng@ump.edu.my (K.F. Chong).

All these support the enhanced aqueous electrolytes movement within electrode materials during electrochemical applications.

Nowadays, the designing of new electrode materials for supercapacitors, using the modified carbon nanotubes and their redox-active composites, is one of the most intensive studies [27–30]. The supercapacitors are crucial devices for energy storage deployments. This is because they exhibit a higher energy density in comparison with conventional capacitors and, at the same time, possess higher power delivery capabilities than batteries [29]. Carbon-based materials store the electrical energy with an electrical double layer mechanism but suffer from low capacitance, therefore, introducing a new component with pseudocapacitance characteristics enhances the capacitive properties of the carbon materials [27,31–34].

Recently the successful functionalization of MWCNTs with electroactive moiety, namely TEMPO radical, was reported, and this material exhibited a capacitance value of 66 F g^{-1} that is 5-times higher than that of non-functionalized MWCNTs (13.5 F g^{-1}) [32]. In another study, Fc was used to functionalize reduced graphene oxide (rGO) as an electrode material for supercapacitors [35]. In addition, rGO was grafted through [35,36] cycloaddition reaction with 4-azidobutylferrocene (AzFc) and its nanocomposite with polyaniline (PANI) was applied as a new battery-type supercapacitor material [37].

In this work, we report the synthesis of ferrocene modified multi-walled carbon nanotubes and the structural, morphological, as well as spectroscopic characterization of the fabricated material. The results of the performed electrochemical studies, namely cyclic voltammetry (CV), galvanostatic charge-discharge (GCD), and electrochemical impedance spectroscopy (EIS), proved that the designed nanomaterials could be successfully used as an effective electrode material for energy storage applications.

2. Experimental section

2.1. Materials

Ferrocenyl amine (Fc-NH$_2$) with purity ≥98%, 1,1′-thiocarbonyldi-2 (1H)-pyridone with purity 97% and all solvents (puriss. p.a.) were purchased from Merck. Amino modified multi-walled carbon nanotubes (MWCNTs-NH$_2$) with purity >95%, -NH$_2$ contents 0.45 wt%, OD: 8–15 nm, ID: 3–5 nm, length: ~50 μm were purchased from Nanostructured & Amorphous Materials, Inc.

2.2. Samples preparation

Preparation of Fc-MWCNTs was performed in two sequential steps: the first one was the synthesis of isothiocyanatoferrocene, and afterward, this compound was used for the modification of amino-functionalized carbon nanotubes.

2.2.1. Synthesis of isothiocyanatoferrocene

To a solution of Fc-NH$_2$ (402 mg, 2 mmol) in anhydrous dichloromethane (20 mL), 1,1′-thiocarbonyldi-2(1H)-pyridone (696 mg, 3 mmol) was added and allowed for 30 min for complete reaction (as monitored by thin-layer chromatography). The reaction mixture was concentrated under reduced pressure, and the residue was purified by silica gel column chromatography using dichloromethane as an eluent to give the isothiocyanatoferrocene as a brownish oil (406 mg, 83% yield). ^{1}H NMR (300 MHz, CDCl$_3$) δ 4.45–4.55 (m, 2H, CH-Fc), 4.33 (s, 5H, Cp-Fc), 4.05–4.20 (m, 2H, CH-Fc).

2.2.2. Synthesis of ferrocene functionalized MWCNTs via a thiourea linker

The suspension of MWCNT-NH$_2$ (2.5 g, NH$_2$ content 0.45 wt%) was sonicated for 5 min in 1% triethylamine in anhydrous dimethylformamide (DMF, 100 mL), followed by addition of isothiocyanatoferrocene (219 mg, 0.90 mmol) as shown in Scheme 1. The suspension was stirred at room temperature for 72 h. The product was isolated by filtration and washed with DMF several times to remove unreacted species. Finally, the thioureaferrocene functionalized MWCNTs were washed with diethyl ether and dried to obtain material in a 92% yield. The prepared material was denoted as Fc-MWCNTs.

2.3. Samples characterization

X-ray photoelectron spectroscopy (XPS) measurements were done using a VG ESCALAB 210 electron spectrometer equipped with monochromatic Al-K$_\alpha$ source (1486.6 eV). The data were calibrated using the binding energy of the C1s transition at 284.6 eV as the internal standard. Fourier transform infrared (FTIR) spectra were performed on a Shimadzu FTIR model 8400S spectrophotometer. The spectra were recorded with a resolution of 8 cm^{-1} from KBr pellets in a ratio of 1:2000 (w/w). ^{1}H NMR spectrum was recorded on a Bruker Corporation 300 MHz spectrometer. ^{1}H NMR chemical shifts δ are reported in ppm referenced to the residual signal of chloroform. Thermogravimetric analysis (TGA) and differential thermogravimetric (DTG) measurements were performed using a TA Instruments DSC Q20 calorimeter with thermobalance (precision ±0.4%; minimal mass 0.02 mg) under an N$_2$ atmosphere with scanning rate 10 K min^{-1}. Scanning Electron Microscopy with Energy-dispersive X-ray spectroscopy (SEM-EDS) was carried out with a scanning electron microscope JEOL-JSM-5600 equipped with energy dispersive X-ray spectrometer OXFORD Link-ISIS-300. The samples were prepared by casting DMF suspension of the sample (sonicated earlier for 10 min) onto a carbon-coated copper
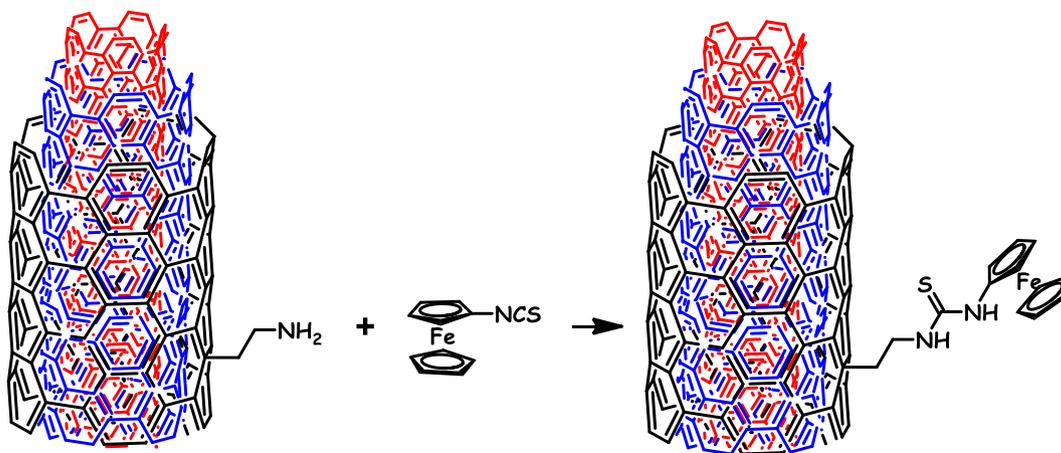
Scheme 1. The route to modification of MWCNT-NH$_2$ with ferrocene.

microgrid (200 mesh) and air-dried for 48 h. Elemental analysis was performed using a CHNS analyzer model Vario EL III Elementar Analysen Systeme GmbH. X-ray Fluorescence Spectroscopy (XRF) was performed using the Bruker Handheld XRF Analyzer equipped with a Silicon Drift Detector (SDD), 50 kV X-ray tube.

2.4. Electrochemical measurements

For electrochemical characterizations, the electrodes were prepared from the active material, carbon black and polyvinylidene fluoride in the weight ratio of 85:10:5. The mixture was cast onto a nickel foam, dried, and then uniaxially pressed at 5 tons. The electrochemical performance was investigated using a three-electrode system, which consists of the active material, Ag/AgCl, and Pt wire (CH Instrument) as a working, reference, and counter electrodes, respectively. The electrochemical data were collected using an AUTOLAB PGSTAT30 electrochemical workstation, equipped with a frequency response analyzer. Cyclic voltammetry (CV) and Galvanostatic charge-discharge (CDC) tests were performed at different scan rates and different current densities, respectively. Electrochemical impedance spectroscopy (EIS) data were collected from 0.01 to 1000 Hz, at open circuit potential (OCP) with a.c. amplitude of 10 mV. All electrochemical measurements were performed using 2 M KOH aqueous electrolyte.

3. Results and discussion

3.1. Structural and morphological analyses

Fig. S1 (Supplementary Information) displays the XPS survey spectrum of MWCNTs surface modified with ferrocene via thiourea linker. The spectra confirm the elemental composition of the fabricated material and the presence of ferrocene moieties at MWCNTs surface. The quantitative data from the XPS analysis are presented in Table 1.

The Fe2p spectrum demonstrates the presence of ferrocene moieties attached to the surface of MWCNTs. It can be deconvoluted into three peaks at 711.6, 718.3, and 725.2 eV (Fig. 1). The peaks at 711.6 and 725.2 eV, with the same full width at half maximum (FWHM), corresponds to $2p_{3/2}$ and $2p_{1/2}$ orbitals, respectively [38]. The additional peak at 718.3 eV corresponds to a shake-up satellite peak characteristic for Fe^{2+} state [39]. Taking into account the atomic ratio of iron to carbon (Fe:C) determined from the XPS and the atomic surface density of 37 atoms/nm^2 for a graphene plane [40], it can be calculated density of grafting with ferrocene as 0.8 molecule/nm^2. The presence of Fe in the

prepared material was also confirmed by XRF and EDS methods (Figs. S2 and S3, Supplementary Materials). The results of the determination of Fe atomic concentrations in the fabricated material, determined by XPS and EDS (see Supplementary Material, Table S1), are consistent (~1%).

The XPS spectra of S2p and N1s reveal that the ferrocene moiety is indeed attached to the MWCNTs surface via a thiourea linker (Fig. 1). In general, the S2p spectrum typically presents a doublet $2p_{3/2}$ and $2p_{1/2}$ as a result of spin-orbit coupling. The fitted experimental S2p spectrum can be deconvoluted into two doublets (Fig. 1). One doublet composed of two peaks at 164.27 and 165.45 eV corresponds to perfect positions observed for C=S band, and distance between them equals 1.18 eV perfectly agrees with an expected value of 1.2 eV for the spin-orbit doublet [41,42]. The second doublet observed in the S2p spectrum reveals the presence of oxidized sulfur in the fabricated materials. However, on the base of quantitative data obtained from XPS analysis, the content of oxidized sulfur in the fabricated material consists ca. 5% of a whole mass. On the base of the atomic concentration of sulfur in the fabricated material determined from XPS, the weight content of this element can be calculated as 0.88% what is consistent with the results of sulfur content determined from elemental analysis 0.55%.

The fitted experimental N1s spectrum (Fig. 1) can be deconvoluted into three peaks at 398.7, 400.4, and 403.3 eV. The first two peaks can be attributed to the N—H groups in a thiourea linker [41]. Wherein as these two peaks differ in their area, most likely, the peak at 400.4 eV contains in its area, besides this one attributed to –NH-C(=S) from a thiourea linker, also the peak attributed to unreacted –NH₂ groups connected with MWCNTs' surface. The presence of the third peak in the N1s spectrum, this at 403.3 eV, most probably results from the residue of DMF not removed during the drying process since it can be strongly adsorbed onto the surface of MWCNTs.

The C1s spectrum is asymmetric, with a long tail extended to higher energy (Fig. 1). The fitted experimental spectrum can be deconvoluted into several peaks with the same values of FWHM. The main peak with the most significant area at 284.5 eV corresponds to the aromatic carbon atoms sp^2 hybridized, carbon atoms connected likely in a graphene and graphite layers and connected in ferrocene rings. The next peak at 285.3 eV can be assigned to the carbon atoms sp^3 hybridized that form C—C and C—H bonds [41,43]. The next peak at 286.2 eV is ascribed to the C=S and C—N bonds in a thiourea linker. While the peaks centering at 287.0 and 287.9 in C1s spectrum are attributed to the carbon atoms connected in carbonyl and carboxyl groups, respectively [32]. Additionally, in the fitted experimental C1s spectrum, a small peak attributed to the double C=C bonds is also visible and at 283.3 eV.

Fig. 2 displays the FTIR spectra of carbon nanotubes functionalized only with amino groups used as a starting material (MWCNTs-NH₂), an amino derivative of ferrocene used for the surface modification (Fc-NH₂) and the final material functionalized with a ferrocene via a thiourea linker (Fc-MWCNTs). The characteristic modes corresponding to the Fc moiety attached to MWCNTs via thiourea linker appear in the Fc-MWCNTs spectrum. The bands at 3399 cm^{-1} in the case of Fc-NH₂ and 3428 cm^{-1} for MWCNTs-NH₂ belong to -NH₂ groups (asymmetric N—H stretching). In the case of Fc-MWCNTs, this band is slightly hypsochromic shifted (3449 cm^{-1}) as a consequence of amide bonds formation in a thiourea linker between Fc moiety and MWCNTs. For the same reason, the -NH₂ deformation modes (at 1491 cm^{-1} for Fc-NH₂ and 1603 for MWCNTs-NH₂) do not appear in the spectrum of Fc-MWCNTs. The weak and broadband at 793 cm^{-1} in the spectrum of Fc-MWCNTs is assigned to the C=S bond vibration in a thiourea linker.

The characteristic FTIR modes for ferrocene appear in the Fc-NH₂ spectrum at 3082, 1094, 1015, and 803 cm^{-1}. These modes are bathochromic shifted in the case of the Fc-MWCNTs spectrum and appear at 2923, 1084, 1010, 793 cm^{-1}, respectively. The shifting of these bands to a lower wavenumber in the Fc-MWCNTs spectrum indicates that the molecular motions of the moieties attached to the carbon

Table 1
Binding energy values, full width at half maximum (FWHM) of peaks, and surface atomic concentrations derived from XPS analysis of Fc-MWCNTs.

Orbital	Position [eV]	FWHM [eV]	Concentration [atom %]
Fe2p$_{3/2}$	711.6	4.278	0.43
Fe2p$_{1/2}$	725.2	4.278	0.22
Fe2p$_{sat}$	718.3	7.000	0.23
N1s	398.7	1.896	0.85
	400.4	1.896	1.10
	403.3	1.896	0.15
S2p$_{3/2}$	164.3	1.873	0.19
S2p$_{1/2}$	165.4	1.873	0.10
S2p$_{3/2}$	168.4	2.520	0.04
S2p$_{1/2}$	169.6	2.520	0.02
O1s	530.4	2.252	1.24
	532.0	2.252	4.11
	534.3	2.252	0.57
C1s	283.3	0.946	2.05
	284.5	0.946	61.2
	285.3	0.946	14.0
	286.2	0.946	7.70
	287.0	0.946	4.20
	288.0	0.946	1.76
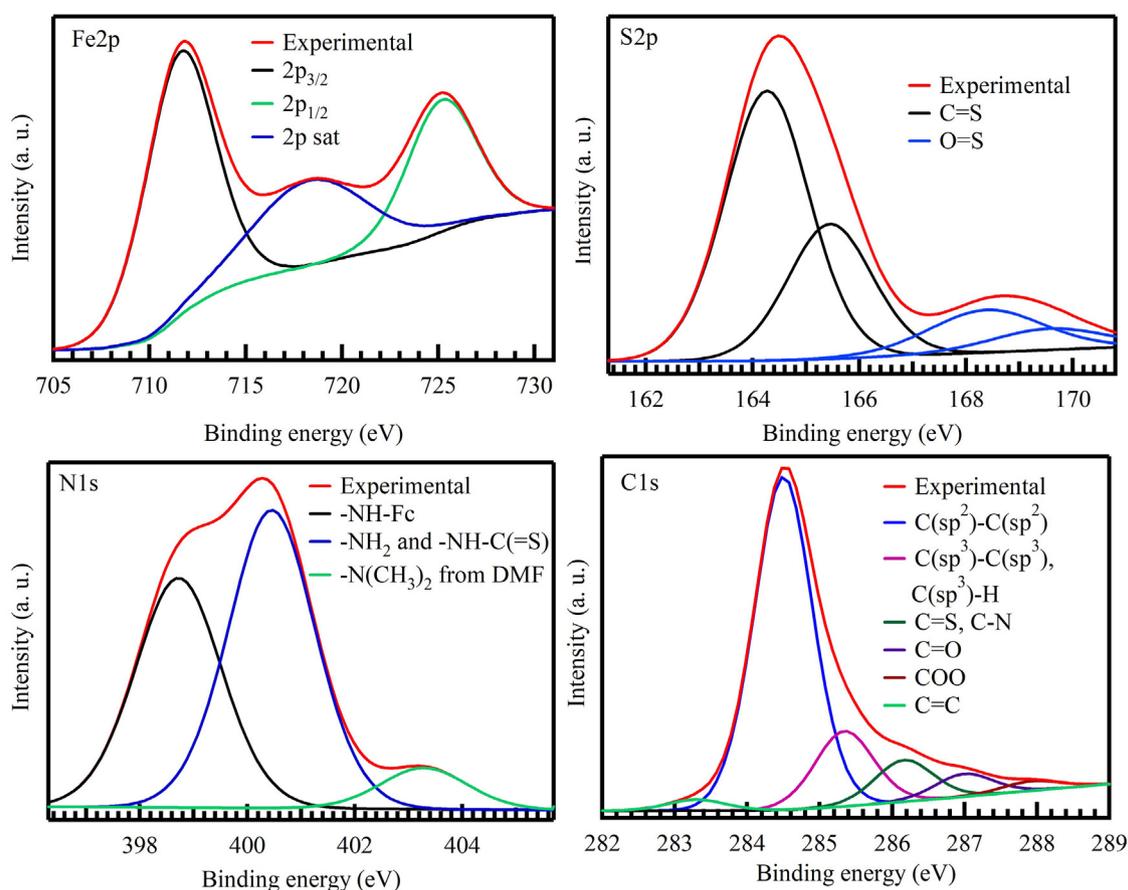
Fig. 1. The XPS spectra of Fe2p, S2p, N1s, and C1s for Fc-MWCNTs.

surface are constrained. The strong band at 1647 cm^{-1} in the spectrum of Fc-MWCNTs is most likely associated to the C—C bonds stretching modes derived from carbon nanotube backbones (1603 cm^{-1}) and ferrocene (1621 cm^{-1}). However, taking into account the positions of these modes in the mentioned spectra, it would be expected that such a combination should be located rather at a lower wavelength. However, as Guan et al. reported, the C—C stretching mode of carbon

nanotube backbones can be upshifted as a result of interactions between π-electrons of the nanotube and the ferrocene moiety [11]. The positive peaks at 2350 cm^{-1} in the spectra result from the presence of carbon dioxide in the spectrophotometer during measurements (not removed from the measuring chamber).

Fig. 3 displays the results of TGA (in the range of 20–950 °C) of Fc-MWCNTs and its starting materials. For comparison, the TGA of the
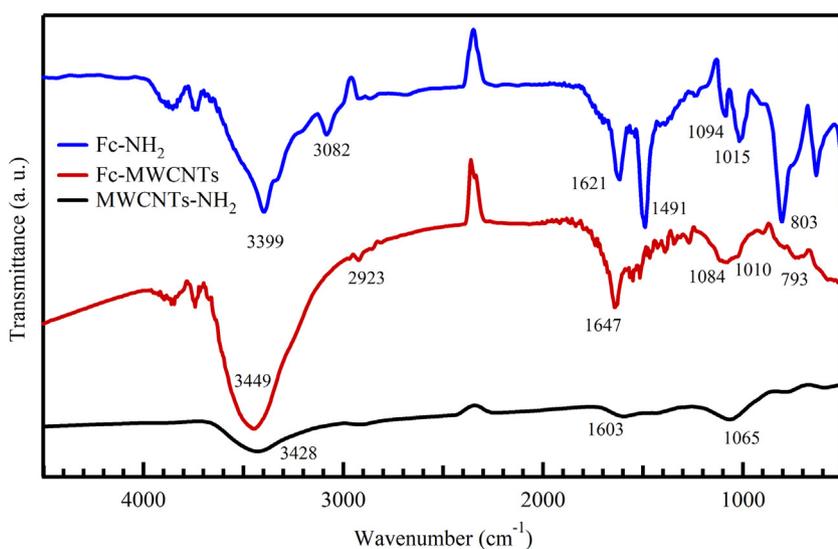
Fig. 2. FTIR spectra recorded for carbon nanotubes functionalized only with amino groups used as a starting material (MWCNTs-NH$_2$), an amino derivative of ferrocene used for the surface modification (Fc-NH$_2$) and the final material functionalized with a ferrocene via a thiourea linker (Fc-MWCNTs).
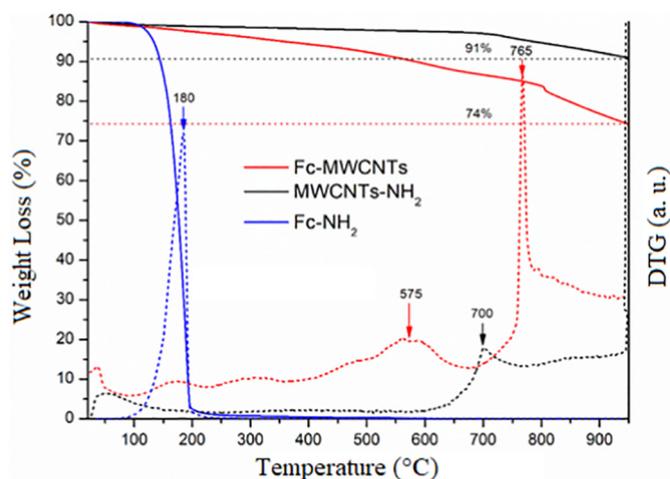
Fig. 3. TGA curves (solid lines) of modified multi-walled carbon nanotubes and ferrocenyl amine used for the modification and corresponding first-derivatives (dotted lines with the same colour) of TGA with respect temperature. The dashed lines show the final mass ratio of the samples after the analyses.

amino derivative of ferrocene, not connected with nanotubes' surface, is also presented. As can be seen, the decomposition of ferrocenyl amine, under the conditions of analysis, is completed below 300 °C, and the maximum weight loss is observed at 180 °C (see the first derivative curve of corresponding TGA curve). Whereas for the carbon nanotubes modified amino groups, the observed weight loss begins above 600 °C with a maximum at 700 °C. After the modification of this material with ferrocene, the decomposition process starts at a significantly lower temperature (150 °C). It is consistent with the results obtained for ferrocene derivatives not connected with the carbon nanotubes surface. During the decomposition of the Fc-MWCNTs multi-steps process occurs, two main stages with maximum weight loss at 575 and 765 °C may be identified. The difference between the final mass (determined

as a percentage of start mass) between MWCNTs-NH$_2$ (91%) and Fc-MWCNTs (74%) confirms the modification of carbon nanotubes with an organic fraction. On the base of this difference, it is possible to estimate a grafting density of ferrocene onto MWCNTs as equals 0.79 mmol/g (see details of calculations in Supplementary Information).

The designed surface modification of carbon nanotubes gave not only the electroactivity of this material but also gave an excellent dispersibility in organic solvents such as DMF. In Fig. 4, images of unmodified and modified with ferrocene MWCNTs dispersed in DMF are displayed. In the case of ferrocene-modified nanomaterials, it is possible to obtain a stable colloidal solution after a short time of sonication that was not possible in the case of MWCNTs-NH$_2$. The morphological differences between MWCNTs-NH$_2$ and Fc-MWCNTs are visible in the presented SEM images (Fig. 4). MWCNTs-NH$_2$ shows aggregates/bundles that are not visible for Fc-MWCNTs. It clearly shows that the designed functionalization of MWCNTs with ferrocene moieties gives dispersibility in DMF and homogeneous of the nanomaterial in a solid-state.

3.2. Electrochemical performance

To study the electrochemical behaviour of the Fc modified MWCNTs, the electrochemical measurements were fully performed through three-electrode configuration using 2 M KOH aqueous electrolyte. The CV curves of MWCNTs-NH$_2$ and Fc-MWCNTs electrodes at a scan rate of 50 mV s^{-1} were presented in Fig. 5a. It can be seen that the CV current of the Fc-MWCNTs electrode has increased in comparison to MWCNTs-NH$_2$, indicating its superiority as a supercapacitor electrode [44]. Besides, the CV curves also maintained a rectangular-like shape with low anodic-cathodic humps (*ca.* −0.5 V) among the low and high scan rates. This indicates the stable electrochemical performance of the Fc-MWCNTs electrode as well as the combination of both electrical double-layer capacitance of MWCNTs and pseudocapacitive behaviour of Fc for charge storage (Fig. 5b) [45,46]. The ferrocene is a reversible redox couple, and it could be oxidized into ferrocenium ion (Fc$^+$) as represented by [7,47] (Fe^{2+}(C$_2$H$_5$)$_2$ ⇌ Fe^{3+}(C$_2$H$_5$)$_2$ + e$^-$). Thus, the redox peaks that appeared in the CVs are assigned to the redox reaction
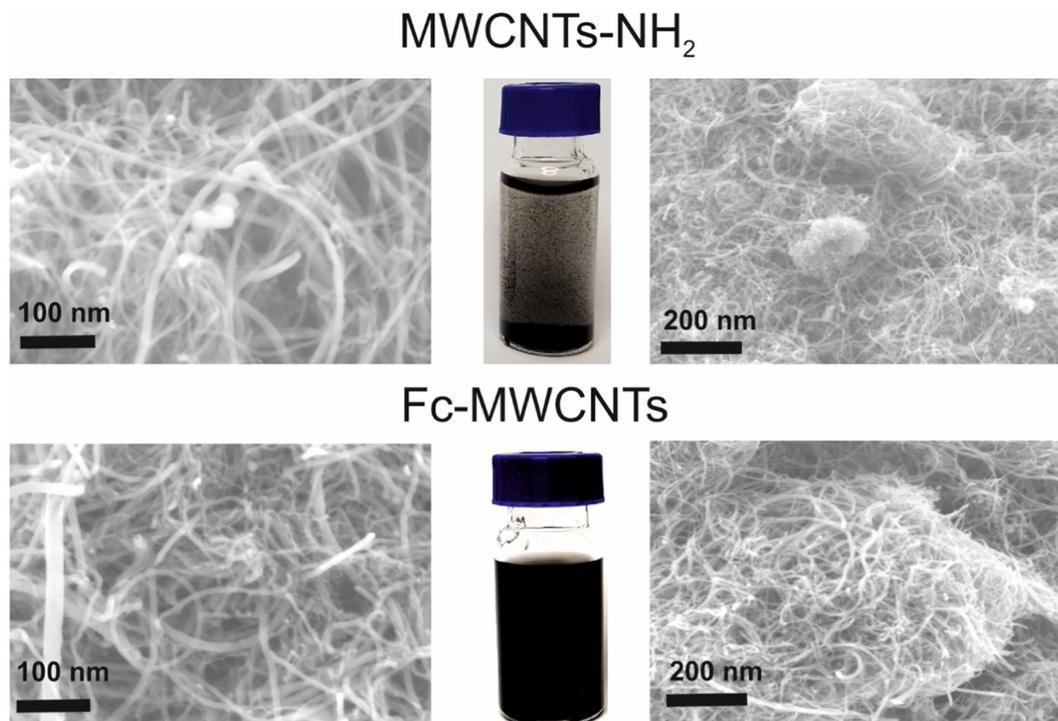
Fig. 4. SEM images of ferrocene-modified multi-walled carbon nanotubes (Fc-MWCNTs) and nanotubes used as a starting material in the modification process (MWCNTs-NH$_2$). The photos between the images show the solutions of these materials in DMF after 5 min of sonication.
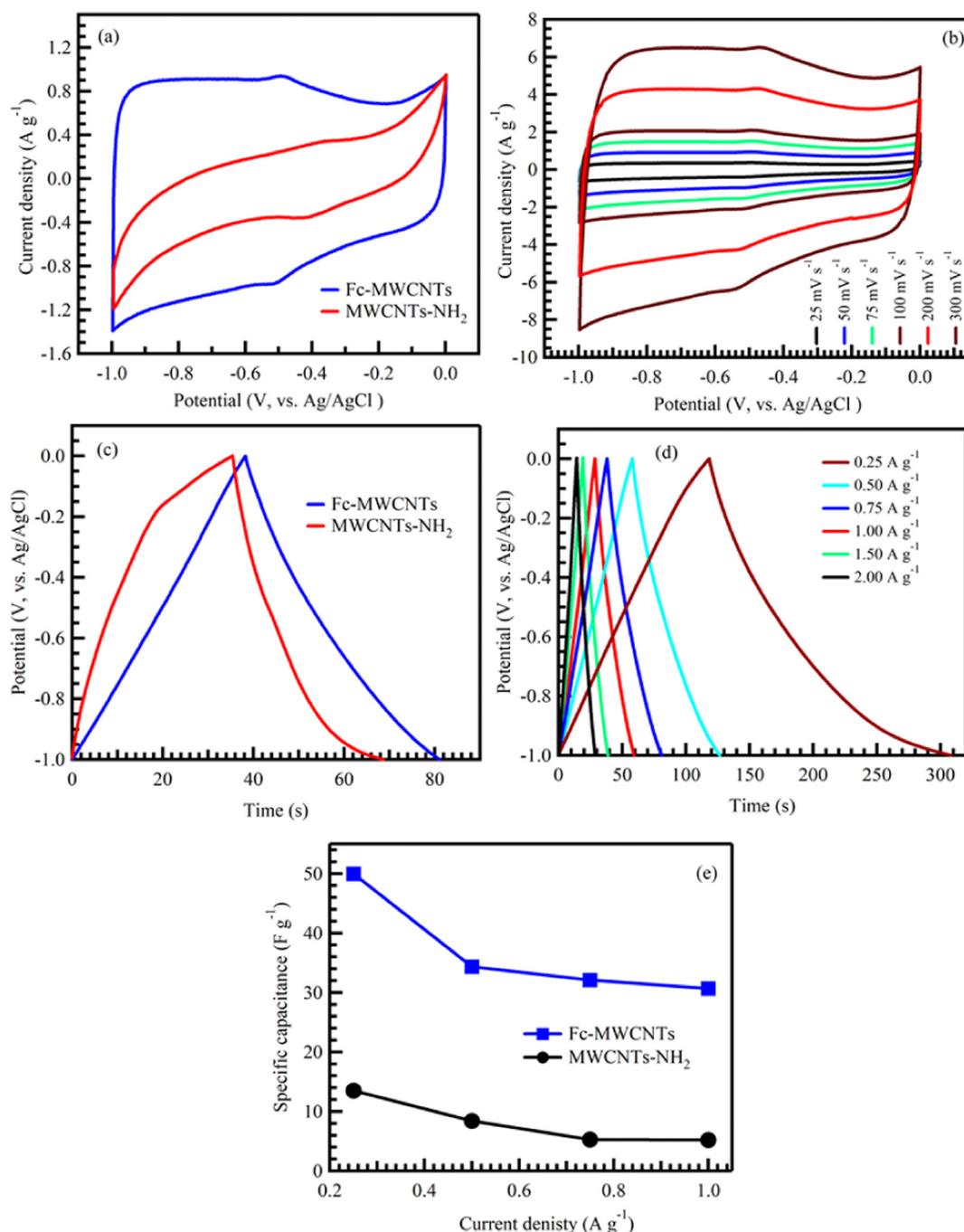
Fig. 5. CV of MWCNTs-NH$_2$ and Fc-MWCNTs at 50 mV s^{-1} (a), CV curves of Fc-MWCNTs at different scan rates (b), GCD curves of MWCNTs-NH$_2$ and Fc-MWCNTs at the current density of 0.75 A g^{-1} (c), GCD curves of Fc-MWCNTs at different current densities (d) and variation of specific capacitance with current densities of MWCNTs-NH$_2$ and Fc-MWCNTs (e).

of Fc/Fc$^+$ system. This is an essential finding in supporting the presence of interaction between Fc and MWCNTs, which enhanced the capacitive response of MWCNTs, as it is confirmed in the earlier part *via* XPS and FTIR studies.

The electrochemical performance of the Fc-MWCNTs electrode was further examined through its charge-discharge properties. A comparison of the GCD curves of MWCNTs-NH$_2$ and Fc-MWCNTs at a current density of 0.75 A g^{-1} is presented in Fig. 5c, which shows the remarkably higher discharge time of Fc-MWCNTs compared to the MWCNTs-NH$_2$ electrode. Additionally, a potential plateau observed in the charging curve of MWCNTs-NH$_2$ from −0.16 to 0 V, and it disappeared in the presence of Fc, which indicates the high-potential of Fc-MWCNTs electrode as an excellent energy storage material. Fig. 5d

depicts the GCD curves of the Fc-MWCNT electrode at various current densities. A slightly changed slope can be observed in the discharge curves, which may be due to the faradaic behaviour that occurs at the electrolyte/electrode interface [37]. This agrees with the CV results; it reveals again the advantages of Fc functionalized on MWCNTs for supercapacitors and highlights the presence of Fc. Furthermore, the specific capacitance of the Fc-MWCNTs electrode has calculated from their GCD curves at different current densities *via* the equation ($C_{sp} = I\Delta t/m\Delta V$) [48,49], and it is displayed in Fig. 5e. The measured specific capacitance of the Fc-MWCNTs electrode at 0.25 A g^{-1} (50 F g^{-1}) is around 4-times higher than that of the MWCNTs-NH$_2$ electrode (13 F g^{-1}).

EIS measurements were taken to analyze the Nyquist and Bode-phase plots in 2 M KOH electrolyte to understand the charge carrier transfer and
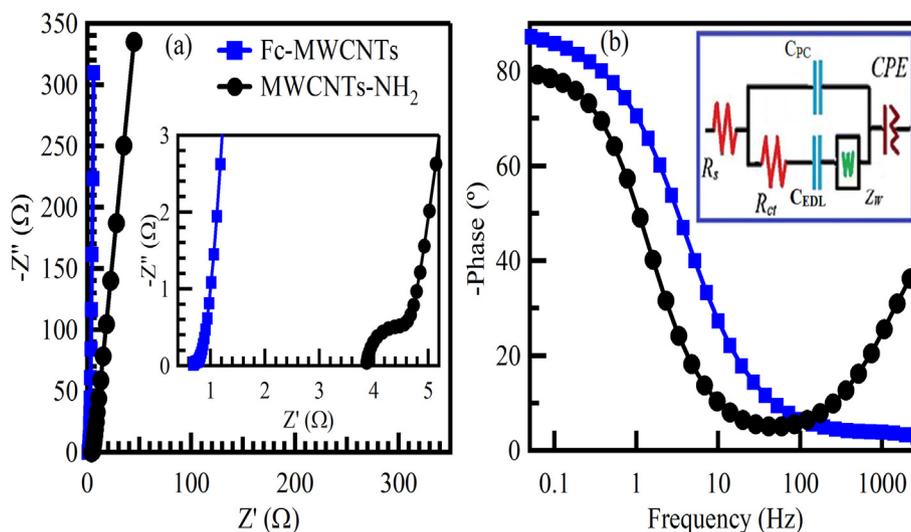
Fig. 6. Nyquist plots (a), the inset is zoomed view of Nyquist plots at the high-frequency region and Bode plots (b) the inset is the equivalent circuit, of MWCNTs-NH$_2$ and Fc-MWCNTs electrodes.

Table 2
Fitting parameters of the experimental impedance data for the electrode materials in 2 M KOH.

Electrode material	Rs (Ω)	R$_{CT}$ (Ω)	C$_{PC}$ (mF)	C$_{EDL}$ (mF)	W (Ω)	S$_E$ (m^2 g^{-1})	τ (s)	Phase ($^\circ$)
Fc-MWCNTs	0.679	0.078	1.33	50.9	1.9	107	0.04	−88.9
MWCNTs-NH$_2$	3.85	0.825	0.3	4.40	0.05	10.5	0.13	−77.3

electrode/electrolyte interfaces in frequencies ranging from 0.01 to 1000 Hz. Nyquist and Bode plots for MWCNTs-NH$_2$ and Fc-MWCNTs are shown in Fig. 6. Nyquist plots consist of two main regions, *i.e.*, semicircle at the high-frequency range and a linear vertical region at low-frequency range (Fig. 6a). The diameter of the semicircular region is an indication of the charge transfer resistance (R$_{CT}$). The linear part is related to diffusion processes. The fitting parameters of the experimental EIS data are listed in Table 2. It was found that R$_{CT}$ value of the Fc-MWCNTs was lower than MWCNTs-NH$_2$, which indicates a more facile charge transfer process across FC-MWCNTs interface [50]. This can be associated to hydrophilicity nature of Fc-MWCNTs, which renders aqueous electrolyte to contact closer to the electrode surface [25,26]. The solution resistance

(R$_S$) of Fc-MWCNTs is 0.679 Ω which is few folds lower than that of pure MWCNTs (3.85 Ω) and other reported value for pristine MWCNTs (3.77 Ω) [32]. It indicates the addition of Fc onto MWCNTs may increase the conductivity of the electrode material [51]. It is worth noting that the Fc-MWCNTs electrode displays a more vertical line than that of the MWCNTs-NH$_2$ electrode, which implies higher capacitive behaviour [52,53] This corroborates well to the CV and GCD results. Similar behaviour was observed for graphene when it is functionalized with iron-containing moieties [33].

The EIS data were further studied to calculate the electrochemically active surface area (S_E, m^2 g^{-1}) of all prepared electrode materials, as reported previously [54–56]. The S_E value of Fc-MWCNTs (107 m^2 g^{-1}) is 10-times larger than that of the MWCNTs-NH$_2$ (10.5 m^2 g^{-1}), indicating more effective contact of the active material with the electrolyte for Fc-MWCNTs. Another important tool for elucidating the nature of the Fc-MWCNTs as active electrode material comes from the study of the relationship among phase angle on the frequency, which can be referred to as the Bode plot [57–59]. From Fig. 6b, the phase angles of Fc-MWCNTs and MWCNTs-NH$_2$ electrodes position close to −88.9° and −77.3° at low frequency, respectively, indicating ideal capacitive behaviour [30,60].
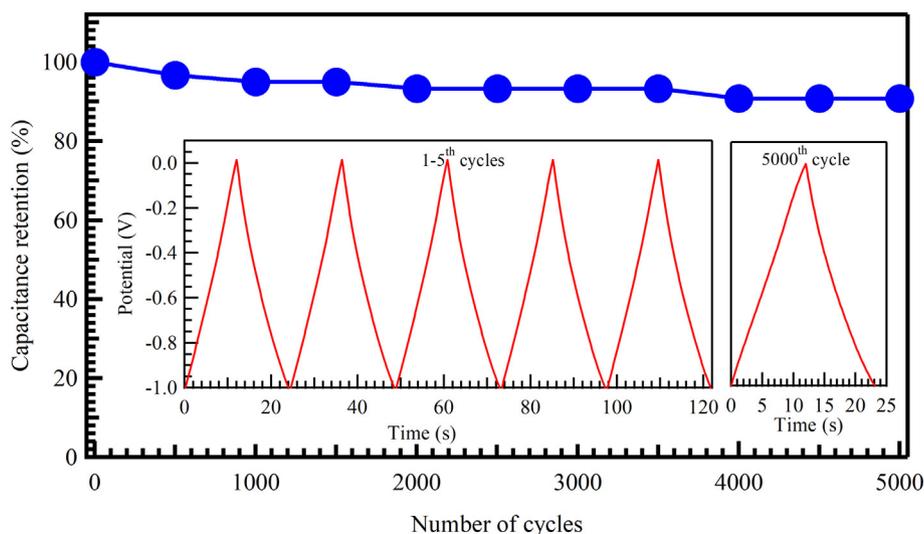
Fig. 7. Cycling stability of the Fc-MWCNTs electrode at a current density of 2 A g^{-1}, the insets show some GCD cycles.

A further advantage of frequency response can be estimated *via* the phase angle of $-45°$, which is corresponding to the minimum time required to discharge all the energy from the device with an efficiency of greater than 50%. The relaxation time (τ) value estimated from the Bode plot using the following equation ($\tau = 1/2\pi f^*$) [49,61–63]. The Fc-MWCNTs electrode exhibits the lower τ value (0.04 s) as compared to that of MWCNTs-NH$_2$ (0.13 s). This indicates excellent electrochemical performance and fast charge-discharge response [64].

Lastly, Fc-MWCNTs exhibits outstanding cycling stability, as shown in Fig. 7 (the insets show some GCD cycles). In particular, 90.8% of its capacitance retained even after 5000 GCD cycles at high current density of 2 A g^{-1}. This is higher than that reported for carbon nanotubes@ tetraferrocenylporphyrin/copper nanohybrid, which showed only 80% after 3000 cycles [65]. Further investigation of the stability was performed by testing the impedance spectra of the same electrode before and after the stability test. Nyquist plots for the Fc-MWCNTs before and after 5000 GCD stability cycles are shown in Fig. S4. It is clearly seen that the electrode shows almost identical behaviour in the low frequency region and slight change at the high frequency region. The fitting parameters of the experimental data show very close value (Table S1), indicating high electrochemical stability of the Fc-MWCNTs electrode. This evidences the long cycle life of the Fc-MWCNTs.

4. Conclusions

Ferrocene functionalized multi-walled carbon nanotubes (Fc-MWCNTs) are successfully synthesized in two steps at low-temperature. Structural, morphological, and spectroscopic investigations confirmed the functionalization process. Fc-MWCNTs were evaluated as a supercapacitor electrode using cyclic voltammetry, galvanostatic charge-discharge, and electrochemical impedance spectroscopy. The Fc-MWCNTs electrode showed excellent capacity retention (90.8% over 5000 cycles) and a specific capacitance of 50 F g^{-1} at 0.25 A g^{-1} compared to the MWCNTs-NH$_2$. Thus, Fc-MWCNTs can be a suitable and promising candidate for future energy storage devices.

CRediT authorship contribution statement

Gomaa A.M. Ali: Conceptualization, Methodology, Investigation, Validation, Writing - original draft. **Elżbieta Megiel:** Conceptualization, Methodology, Writing - original draft. **Piotr Cieciórski:** Visualization, Methodology. **Mohammad R. Thalji:** Methodology, Validation. **Jan Romański:** Conceptualization, Visualization, Methodology, Investigation. **H. Algarni:** Writing - review & editing. **Kwok Feng Chong:** Conceptualization, Supervision, Writing - review & editing.

Declaration of competing interest

The authors declare that they have no known competing financial interests or personal relationships that could have appeared to influence the work reported in this paper.

Acknowledgments

Appendix A. Supplementary data

Supplementary data to this article can be found online at https://doi.org/10.1016/j.molliq.2020.114064.

References

[1] J.M. Marulanda, Electronic Properties of Carbon Nanotubes, BoD–Books on Demand, 2011.
[2] J.-S. Ye, F.-S. Sheu, Functionalization of CNTs: new routes towards the development of novel electrochemical sensors, Curr. Nanosci. 2 (2006) 319–327.
[3] E. Megiel, Surface modification using TEMPO and its derivatives, Adv. Colloid Interf. Sci. 250 (2017) 158–184.
[4] A. Barhoum, A.E. Shalan, S.I. El-Hout, G.A.M. Ali, S.M. Abdelbasir, E.S. Abu Serea, A.H. Ibrahim, K. Pal, A broad family of carbon nanomaterials: classification, properties, synthesis, and emerging applications, in: A. Barhoum, M. Bechelany, A. Makhlouf (Eds.), Handbook of Nanofibers, Springer International Publishing, Cham 2019, pp. 1–40.
[5] H. Sadegh, G.A.M. Ali, A.S.H. Makhlouf, K.F. Chong, N.S. Alharbi, S. Agarwal, V.K. Gupta, MWCNTs-Fe$_3$O$_4$ nanocomposite for hg(II) high adsorption efficiency, J. Mol. Liq. 258 (2018) 345–353.
[6] A. Rabti, N. Raouafi, A. Merkoçi, Bio (sensing) devices based on ferrocene–functionalized graphene and carbon nanotubes, Carbon 108 (2016) 481–514.
[7] Y. Wang, E.I. Rogers, R.G. Compton, The measurement of the diffusion coefficients of ferrocene and ferrocenium and their temperature dependence in acetonitrile using double potential step microdisk electrode chronoamperometry, J. Electroanal. Chem. 648 (2010) 15–19.
[8] K. Kaniewska, J. Romański, M. Karbarz, Oxidation of ferrocenemethanol grafted to a hydrogel network through cysteine for triggering volume phase transition, RSC Adv. 3 (2013) 23816–23823.
[9] K. Marcisz, M. Mackiewicz, J. Romanski, Z. Stojek, M. Karbarz, Significant, reversible change in microgel size using electrochemically induced volume phase transition, Appl. Mater. Today 13 (2018) 182–189.
[10] X. Yang, Y. Lu, Y. Ma, Y. Li, F. Du, Y. Chen, Noncovalent nanohybrid of ferrocene with single-walled carbon nanotubes and its enhanced electrochemical property, Chem. Phys. Lett. 420 (2006) 416–420.
[11] L. Guan, Z. Shi, M. Li, Z. Gu, Ferrocene-filled single-walled carbon nanotubes, Carbon 43 (2005) 2780–2785.
[12] D.M. Guldi, M. Marcaccio, D. Paolucci, F. Paolucci, N. Tagmatarchis, D. Tasis, E. Vázquez, M. Prato, Single-Wall carbon nanotube–ferrocene nanohybrids: observing intramolecular electron transfer in functionalized SWNTs, Angew. Chem. Int. Ed. 42 (2003) 4206–4209.
[13] O. Reynes, C. Bucher, J.-C. Moutet, G. Royal, E. Saint-Aman, E.-M. Ungureanu, Electrochemical sensing of anions by redox-active receptors built on the ferrocenyl cyclam framework, J. Electroanal. Chem. 580 (2005) 291–299.
[14] A. Goel, N. Brennan, N. Brady, P.T. Kenny, Electrochemical recognition of anions by 1,1′-N,N′-ferrocenoylbisamino acid esters, Biosens. Bioelectron. 22 (2007) 2047–2050.
[15] Q.-Y. Cao, Y.-M. Han, P.-S. Yao, W.-F. Fu, Y. Xie, J.-H. Liu, A new ferrocene–anthracene dyad bearing amide and triazolium donors for dual-signaling sensing to anions, Tetrahedron Lett. 55 (2014) 248–251.
[16] A. Caballero, N.G. White, P.D. Beer, A ferrocene imidazolium-based macrocycle as an electrochemical chemosensor for halide anions, CrystEngComm 16 (2014) 3694–3698.
[17] H. Miyaji, S.R. Collinson, I. Prokeš, J.H. Tucker, A ditopic ferrocene receptor for anions and cations that functions as a chromogenic molecular switch, Chem. Commun. (2003) 64–65.
[18] M. del Carmen González, F. Otón, A. Espinosa, A. Tárraga, P. Molina, A densely decorated disubstituted ferrocene as an ion-pair recognition receptor, Chem. Commun. 49 (2013) 9633–9635.
[19] M.a. Alfonso, A. Tárraga, P. Molina, A bisferrocene-benzobisimidazole triad as a multichannel ditopic receptor for selective sensing of hydrogen sulfate and mercury ions, Org. Lett. 13 (2011) 6432–6435.
[20] M. Alfonso, A. Espinosa Ferao, A. Tarraga, P. Molina, Electrochemical and fluorescent ferrocene-imidazole-based dyads as ion-pair receptors for divalent metal cations and oxoanions, Inorg. Chem. 54 (2015) 7461–7473.
[21] C. Arivazhagan, R. Borthakur, S. Ghosh, Ferrocene and triazole-appended rhodamine based multisignaling sensors for Hg^{2+} and their application in live cell imaging, Organometallics 34 (2015) 1147–1155.
[22] P. Molina, A. Tárraga, M. Alfonso, Ferrocene-based multichannel ion-pair recognition receptors, Dalton Trans. 43 (2014) 18–29.
[23] H. Miyaji, D.-S. Kim, B.-Y. Chang, E. Park, S.-M. Park, K.H. Ahn, Highly cooperative ion-pair recognition of potassium cyanide using a heteroditopic ferrocene-based crown ether–trifluoroacetylcarboxanilide receptor, Chem. Commun. (2008) 753–755.
[24] M. Zaleskaya, D. Jagleniec, M. Karbarz, Ł. Dobrzycki, J. Romański, Squaramide based ion pair receptors possessing ferrocene as a signaling unit, Inorg. Chem. Front. 7 (2020) 972–983.
[25] R. Pietschnig, Polymers with pendant ferrocenes, Chem. Soc. Rev. 45 (2016) 5216–5231.
[26] B.M. Maciejewska, A. Warowicka, A. Baranowska-Korczyc, K. Załęski, T. Zalewski, K.K. Kozioł, S. Jurga, Magnetic and hydrophilic MWCNT/Fe composites as potential T2-weighted MRI contrast agents, Carbon 94 (2015) 1012–1020.

[27] G.A.M. Ali, E.Y. Lih Teo, E.A.A. Aboelazm, H. Sadegh, A.O.H. Memar, R. Shahryari-Ghoshekandi, K.F. Chong, Capacitive performance of cysteamine functionalized carbon nanotubes, Mater. Chem. Phys. 197 (2017) 100–104.

[28] G.A.M. Ali, H. Sadegh, M.M. Yusoff, K.F. Chong, Highly stable symmetric supercapacitor from cysteamine functionalized multi-walled carbon nanotubes operating in a wide potential window, Mater. Today: Proc. 16 (2019) 2273–2279.

[29] A. Ghosh, Y.H. Lee, Carbon-based electrochemical capacitors, ChemSusChem 5 (2012) 480–499.

[30] B. Pandit, S.S. Karade, B.R. Sankapal, Hexagonal VS_2 anchored MWCNTs: first approach to design flexible solid-state symmetric supercapacitor device, ACS Appl. Mater. Interfaces 9 (2017) 44880–44891.

[31] G.A.M. Ali, O.A. Habeeb, H. Algarni, K.F. Chong, CaO impregnated highly porous honeycomb activated carbon from agriculture waste: symmetrical supercapacitor study, J. Mater. Sci. 54 (2018) 683–692.

[32] G.A.M. Ali, E. Megiel, J. Romański, H. Algarni, K.F. Chong, A wide potential window symmetric supercapacitor by TEMPO functionalized MWCNTs, J. Mol. Liq. 271 (2018) 31–39.

[33] P.E. Marina, G.A.M. Ali, L.M. See, E.Y.L. Teo, E.-P. Ng, K.F. Chong, In situ growth of redox-active iron-centered nanoparticles on graphene sheets for specific capacitance enhancement, Arab. J. Chem. 12 (2019) 3883–3889.

[34] S. Pilathottathil, T. Kannan Kottummal, M.S. Thayyil, P. Mahadevan Perumal, J. Ambichi Purakakath, Inorganic salt grafted ionic liquid gel electrolytes for efficient solid state supercapacitors: electrochemical and dielectric studies, J. Mol. Liq. 264 (2018) 72–79.

[35] R. Teimuri-Mofrad, R. Hadi, H. Abbasi, Synthesis and characterization of ferrocene-functionalized reduced graphene oxide nanocomposite as a supercapacitor electrode material, J. Organomet. Chem. 880 (2019) 355–362.

[36] R. Teimuri-Mofrad, R. Hadi, H. Abbasi, R. Fadakar Bajeh Baj, Synthesis, characterization and electrochemical study of carbon nanotube/chitosan-ferrocene nanocomposite electrode as supercapacitor material, J. Electron. Mater. 48 (2019) 4573–4581.

[37] R. Hadi, H. Abbasi, E. Payami, I. Ahadzadeh, R. Teimuri-Mofrad, Synthesis, characterization and electrochemical properties of 4-azidobutylferrocene-grafted reduced graphene oxide-polyaniline nanocomposite for supercapacitor applications, ChemistrySelect 5 (2020) 575–583.

[38] A.P. Grosvenor, B.A. Kobe, M.C. Biesinger, N.S. McIntyre, Investigation of multiplet splitting of Fe 2p XPS spectra and bonding in iron compounds, Surf. Interface Anal. 36 (2004) 1564–1574.

[39] P.C. Graat, M.A. Somers, Simultaneous determination of composition and thickness of thin iron-oxide films from XPS Fe 2p spectra, Appl. Surf. Sci. 100 (1996) 36–40.

[40] J. Cambedouzou, P. Landois, S. Rouzière, M. Pinault, C. Mocuta, L. Hennet, D. Thiaudière, M. Mayne-L'Hermite, P. Launois, Anomalous thermal expansion of γ-iron nanocrystals inside multiwalled carbon nanotubes, Phys. Rev. B 88 (2013) 081402.

[41] Ü.T. Yılmaz, E. Çalık, D. Uzun, F. Karipcin, H. Yılmaz, Selective and sensitive determination of tannic acid using a 1-benzoyl-3-(pyrrolidine) thiourea film modified glassy carbon electrode, J. Electroanal. Chem. 776 (2016) 1–8.

[42] M.E. Labib, J.H. Thomas, D.D. Embert, The effect of heat treatment on sulfur in an electrically-conductive carbon black, Carbon 22 (1984) 445–451.

[43] H.L. Tan, A. Du, R. Amal, Y.H. Ng, Decorating platinum on nitrogen-doped graphene sheets: control of the platinum particle size distribution for improved photocatalytic H_2 generation, Chem. Eng. Sci. 194 (2019) 85–93.

[44] T.N. Vinuth Raj, P.A. Hoskeri, H.B. Muralidhara, C.R. Manjunatha, K. Yogesh Kumar, M.S. Raghu, Facile synthesis of perovskite lanthanum aluminate and its green reduced graphene oxide composite for high performance supercapacitors, J. Electroanal. Chem. 858 (2020), 113830.

[45] J. Ju, M. Kim, S. Jang, Y. Kim, Y. Choi, S.-H. Baeck, S.E. Shim, 3D in-situ hollow carbon fiber/carbon nanosheet/$Fe_3C@Fe_3O_4$ by solventless one-step synthesis and its superior supercapacitor performance, Electrochim. Acta 252 (2017) 215–225.

[46] C. Long, T. Wei, J. Yan, L. Jiang, Z. Fan, Supercapacitors based on graphene-supported iron nanosheets as negative electrode materials, ACS Nano 7 (2013) 11325–11332.

[47] C.O. Laoire, E. Plichta, M. Hendrickson, S. Mukerjee, K.M. Abraham, Electrochemical studies of ferrocene in a lithium ion conducting organic carbonate electrolyte, Electrochim. Acta 54 (2009) 6560–6564.

[48] M.R. Thalji, G.A.M. Ali, H. Algarni, K.F. Chong, Al^{3+} ion intercalation pseudocapacitance study of $W_{18}O_{49}$ nanostructure, J. Power Sources 438 (2019), 227028.

[49] G.A.M. Ali, Recycled MnO_2 nanoflowers and graphene nanosheets for low-cost and high performance asymmetric supercapacitor, J. Electron. Mater. (2020)https://doi.org/10.1007/s11664-020-08268-7 (doi: 10.1007/s11664-11020-08268-11667).

[50] G. Pan, F. Cao, Y. Zhang, X. Xia, N-doped carbon nanofibers arrays as advanced electrodes for supercapacitors, J. Mater. Sci. Technol., https://doi.org/10.1016/j.jmst.2019.10.004(2019).

[51] Z. Xie, H.L. Tan, X. Wen, Y. Suzuki, A. Iwase, A. Kudo, R. Amal, J. Scott, Y.H. Ng, The importance of the interfacial contact: is reduced graphene oxide always an enhancer in photo(electro)catalytic water oxidation? ACS Appl. Mater. Interfaces 11 (2019) 23125–23134.

[52] Y. Zhang, W.W. Guo, T.X. Zheng, Y.X. Zhang, X. Fan, Engineering hierarchical diatom@CuO@MnO_2 hybrid for high performance supercapacitor, Appl. Surf. Sci. 427 (2018) 1158–1165.

[53] G.A.M. Ali, M.R. Thalji, W.C. Soh, H. Algarni, K.F. Chong, One-step electrochemical synthesis of MoS_2/graphene composite for supercapacitor application, J. Solid State Electrochem. 24 (2019) 25–34.

[54] S. Chou, F. Cheng, J. Chen, Electrodeposition synthesis and electrochemical properties of nanostructured γ-MnO_2 films, J. Power Sources 162 (2006) 727–734.

[55] M.R. Thalji, G.A.M. Ali, S.P. Lee, K.F. Chong, Solvothermal synthesis of reduced graphene oxide as electrode material for supercapacitor application, Chem. Adv. Mater. 4 (3) (2019) 17–26.

[56] G.A.M. Ali, M.M. Yusoff, E.R. Shaaban, K.F. Chong, High performance MnO_2 nanoflower supercapacitor electrode by electrochemical recycling of spent batteries, Ceram. Int. 43 (2017) 8440–8448.

[57] B. Pandit, B.R. Sankapal, Highly conductive energy efficient electroless anchored silver nanoparticles on MWCNTs as a supercapacitive electrode, New J. Chem. 41 (2017) 10808–10814.

[58] T. Purkait, G. Singh, D. Kumar, M. Singh, R.S. Dey, High-performance flexible supercapacitors based on electrochemically tailored three-dimensional reduced graphene oxide networks, Sci. Rep. 8 (2018) https://doi.org/10.1038/s41598-017-18593-3.

[59] G.A.M. Ali, A. Divyashree, S. Supriya, K.F. Chong, A.S. Ethiraj, M.V. Reddy, H. Algarni, G. Hegde, Carbon nanospheres derived from Lablab purpureus for high performance supercapacitor electrodes: a green approach, Dalton Trans. 46 (2017) 14034–14044.

[60] S. Sankar, A.T.A. Ahmed, A.I. Inamdar, H. Im, Y.B. Im, Y. Lee, D.Y. Kim, S. Lee, Biomass-derived ultrathin mesoporous graphitic carbon nanoflakes as stable electrode material for high-performance supercapacitors, Mater. Des. 169 (2019), 107688.

[61] G.S. Gund, D.P. Dubal, B.H. Patil, S.S. Shinde, C.D. Lokhande, Enhanced activity of chemically synthesized hybrid graphene oxide/Mn_3O_4 composite for high performance supercapacitors, Electrochim. Acta 92 (2013) 205–215.

[62] G.A.M. Ali, M.M. Yusoff, H. Algarni, K.F. Chong, One-step electrosynthesis of MnO_2/rGO nanocomposite and its enhanced electrochemical performance, Ceram. Int. 44 (2018) 7799–7807.

[63] G.A.M. Ali, S.A.A. Manaf, D, A, K.F. Chong, G. Hegde, Superior supercapacitive performance in porous nanocarbons, J. Energy Chem. 25 (2016) 734–739.

[64] G.A.M. Ali, S. Supriya, K.F. Chong, E.R. Shaaban, H. Algarni, T. Maiyalagan, G. Hegde, Superior supercapacitance behavior of oxygen self-doped carbon nanospheres: a conversion of Allium cepa peel to energy storage system, Biomass Convers. Bioref. (2019) https://doi.org/10.1007/s13399-019-00520-3.

[65] R. Teimuri-Mofrad, R. Hadi, H. Abbasi, E. Payami, S. Neshad, Green synthesis of carbon nanotubes@tetraferrocenylporphyrin/copper nanohybrid and evaluation of its ability as a supercapacitor, J. Organomet. Chem. 899 (2019), 120915.